Dynamic analysis of metamaterials for industrial applications: numerical predictions and experimental results

Dynamic analysis of metamaterials for industrial applications: numerical predictions and experimental results

A.P. Daga, L. Viale, D. Agabiti, A. Fasana, L. Garibaldi
Department of Mechanical and Aerospace Engineering, Politecnico di Torino,
Corso Duca degli Abruzzi 24, 10129 Torino, Italy
e-mail: **alessandro.daga@polito.it**

Abstract
Metamaterials hold promise for enhancing vibroacoustic performance in sectors like automotive, aerospace, and infrastructure. Advanced design methodologies enable these materials to create targeted bandgaps and suppress unwanted waves and vibrations. This research focuses on analyzing vibroacoustic metamaterials, emphasizing the bandgap phenomenon through numerical predictions and experiments. It examines how variations in geometry, size, periodicity, and material properties affect the bandgap. The study compares numerical simulations with experimental results to validate the design process. By manipulating pattern parameters, the research aims to optimize bandgap characteristics of a metal plate for industrial applications, ensuring the design's reliability and effectiveness for practical use.

1 Introduction

The study of noise, vibration, and harshness (NVH) is crucial in vehicles to enhance passenger safety and comfort. For traditional internal combustion engine (ICE) vehicles, lightweight design solutions are increasingly sought after to reduce emissions and improve factors such as fuel efficiency, tire mileage, and overall vehicle performance [1]. Additionally, as the industry transitions from conventional ICE vehicles to hybrid and electric vehicles, the sources and ranges of noise frequencies will also change.

To address noise, vibration, and weight issues in vehicles, one of the latest solutions in the NVH field is the use of metamaterials. These engineered materials not only reduce noise and vibration but also help decrease vehicle weight. Metamaterials possess unique properties not found in natural materials, which can be controlled through the design of their macro units. Hence the definition of “meta-materials”, with the suffix "meta-" meaning "beyond" or "transitional" in Greek.

NVH metamaterials, formed by the periodic arrangement of unit cells, commonly consist of local resonators realized on top of a host structure (usually a metal surface). These materials feature a stopband, a frequency region where elastic wave transmission is inhibited, reducing noise and vibration. Such bandgap can be achieved through local resonance or Bragg scattering (i.e., local resonance bandgaps obtained through multiple scattering and interference effects occurring between periodic elements in a propagation medium). Local resonance attenuates elastic waves with wavelengths comparable to the unit cell's length. For frequencies under 1 kHz using Bragg scattering, either a unit cell with extremely low specific stiffness or an unrealistically large unit cell is required [2]. Hence, in the automotive field, the local resonance mechanism is more suitable as it can attenuate waves with wavelengths two orders of magnitude greater than the lattice constant of the metamaterial [3]. This makes local resonance metamaterials especially well-suited for low-frequency applications, where conventional NVH solutions require heavy and bulky systems.

The bandgap in metamaterials is achieved through the out-of-phase vibrations of local resonators, which interfere with propagating sound or vibration waves at frequencies similar to the resonator's natural

frequencies [4]. The stopband can be tuned by altering the geometric characteristics of the resonant structure, allowing for a wider frequency range of NVH attenuation.

Many examples of vibration attenuation applications can be found in the literature. Some or the most interesting are reported in Table 1 below and summarized hereinafter.

Table 1 – Brief literature review for vibration attenuation exploiting local resonator metamaterials suitable for NVH applications with corresponding references.

Resonator unit cell design	**Resonator material**	**Evaluated bandgap [Hz] (band size [Hz])**	**Unit cell size [mm]**	**Ref.**
Composite sandwich with spiral resonators	SCFRPs & CCFRPs	490-600 (110)	20 x 25	[2]
Torsional local resonators	NA	87-90 (3)	NA	[4]
Hollow parallelepiped	photopolymer	350-390 (40)	30 x 30	[5]
Single cantilever beam	PMMA	490-540 (50)	25 x 25	[6]
Cantilever beam with endpoint mass	PMMA (body), steel (endpoint mass)	292 -323 (31)	35 x 20	[7]
Z-shaped frame	Aluminum	178-198 (20) & 198-225 (27)	65 x 65	[8]
T-shaped	Aluminum	615-635 (20)	40 x 40	[9]

In particular, in [2] the proposed application involves using 3D printing technology to manufacture metamaterials from carbon fiber-reinforced plastics (SCFRPs) and continuous carbon fiber-reinforced plastics (CCFRPs). The unit cell of the metamaterial consists of a 20 x 25 mm plate with a spiral resonator comprising a mass and spiral spring. The unit cell features a sandwich structure with stiff skin plates and a hollow core. A stop band between 480 and 600 Hz was identified from a unit cell analysis dispersion diagram. A metamaterial plate with periodically displaced unit cells was also analyzed via Finite Element Method (FEM) simulations. Frequency responses obtained for x, y, and z directional inputs and outputs proved a decreased transmissibility in the bandgap region. Finally, experimental testing involved hanging the metamaterial plate from an elastic thread, placing accelerometers at its ends, and exciting it with a shaker at the input point. The results generally aligned with numerical analysis expectations, although the observed attenuation was slightly lower.

In [4] a metamaterial unit cell composed of a torsional local resonator periodically arranged on a beam was studied. Analytical methods using Timoshenko beam theory and Bloch's theorem were employed to evaluate the dispersion relation. For the numerical model, the BEAM188 property was applied to the host beam, and the resonant structure was modeled using MASS21 and COMBIN14 elements. The analysis revealed a stopband between 86.8Hz and 89.5Hz. Increasing the torsional stiffness widened and shifted the band gap to higher frequencies. Finite element method (FEM) analysis of a finitely long model with different torsional local resonators showed three regions of significantly reduced transmittance, aligning with the bandgaps of the resonators. The stopband starts before the local resonant frequency and ends at the torsional resonator's local resonant frequency.

A metamaterial unit cell consisting of a host structure and a hollow parallelepiped local resonator was proposed in [5]. The host structure was made of mild steel with a thickness of 2.4 mm, while the local resonator was made from a photopolymer, but could also be manufactured through injection molding or vacuum casting. By varying the pin diameter, different bandgaps can be achieved, allowing material distribution changes between the spring and mass sections. This was highlighted both with a unit cell bandgap analysis and by a numerical simulation of a metamaterial plate showing significant vibration attenuation for various cases with different internal diameters. The bending modes of the untreated host

structure were attenuated by at least two orders of magnitude with a 20% mass increase, indicating effective vibration reduction.

In [6] a single cantilever beam local resonator metamaterial was studied, made of PMMA, with a mass at its end and horizontal support linking it to a duct host structure. The duct was modeled as rectangular and non-fluid loaded to reduce computational costs. The sequential configuration, which combined different types of resonators along the duct, presented a compelling solution for NVH applications in the automotive field. It achieved a broader frequency range of attenuation compared to configurations with only one type of resonator, making it potentially more effective for reducing noise and vibration across various frequencies.

A similar local resonator made of a cantilever beam (in PMMA) with a steel endpoint mass was covered by [7]. Nevertheless, a more complex host structure with multiple transmission paths (unlike the 1-d transmission path of [6]) was considered, resembling a scenario where a section of a vehicle body is affected by a shock absorber. Unlike other solutions, this metamaterial application required minimal coverage over the host structure, resulting in lower added mass, making it suitable for compact and lightweight applications. The average mitigation achieved is 6.8 dB with a mass increase of only 2.4%.

In [8] the proposed metamaterial unit cell featured a thin homogeneous plate host structure and a local resonator composed of a square z-shaped frame, two trapezoidal plates, and an M4 screw. The frame was made of aluminum, while the plates were made of structural steel and aluminum. Numerical simulation of the unit cell's band structure revealed two complete bandgaps between 178-198 Hz and 198-225 Hz. Simulating a full plate with sinusoidal excitation at 185 Hz and 210 Hz, frequencies within the stop band, showed significant modal displacement reduction and vibration attenuation in the bandgap region.

Finally, in [9] a narrow beam with a wide, upward-bent final section was proposed. For compactness and easier fabrication, such a resonator was achieved through punching and bending aluminum alloy EN AW-6082 samples. Using an inverse modeling approach for FEM band structure analysis under the assumptions of an infinite periodic system and low damping, a stop band between 615 Hz and 635 Hz was identified.

When a full plate structure was modeled, the addition of the local resonator increased the mass by about 20%. The stop band shifted to 580 – 610 Hz, lower than expected. Experimental validation of the full plate confirmed a bandgap in the 500 – 700 Hz range, which was wider but less deep than initially calculated.

The ease of manufacturing and compactness of this resonator make it a promising option for automotive NVH applications in mass production, leading to its selection for the further analyses proposed in this.

In particular, in section 2 the bandgap for an infinite periodic plate metamaterial similar to that in [9] was re-computed, so as to validate the procedure. Then, a simplified version of such a metamaterial was defined for further studies involving the analysis of the stopband with respect to topological considerations.

In section 3 FEM simulations of a real, finite plate were conducted on different plate sizes, while in section 4 experimental measurements were used to test the goodness of the finite plate models in predicting the stop band. Conclusions will be drawn in section 5.

2 Bandgap estimation: infinite periodic metamaterial

Testing metamaterials typically involves starting with a unit cell FEM analysis to determine the dispersion curves and identify the bandgap regions. By applying Bloch's theorem enforcing periodicity at the boundaries and solving the resulting eigenvalue problem for ω along the Irreducible Brillouin Contour, the frequency regions where elastic wave transmission is inhibited are determined, indicating effective noise and vibration attenuation capabilities of the metamaterial [10,11,12].

Such a procedure was first applied to the metamaterial proposed in [9] so as to validate routine developed in COMSOL Multiphysics. The analysis was later simplified to consider a flat t-shape resonator alone.

2.1 Procedure validation

In [9] the considered metamaterial consists of a unitary cell made by a punched and bent T-shape resonator made of 0.5 mm thick aluminum plate, mounted (i.e., glued) on 0.7 mm steel plate host structure. In that study, taken as a reference, the dispersion diagram evaluated along the Irreducible Brillouin contour from O to B according to O → A → B → O → C → B was obtained, as shown in Figure 1.

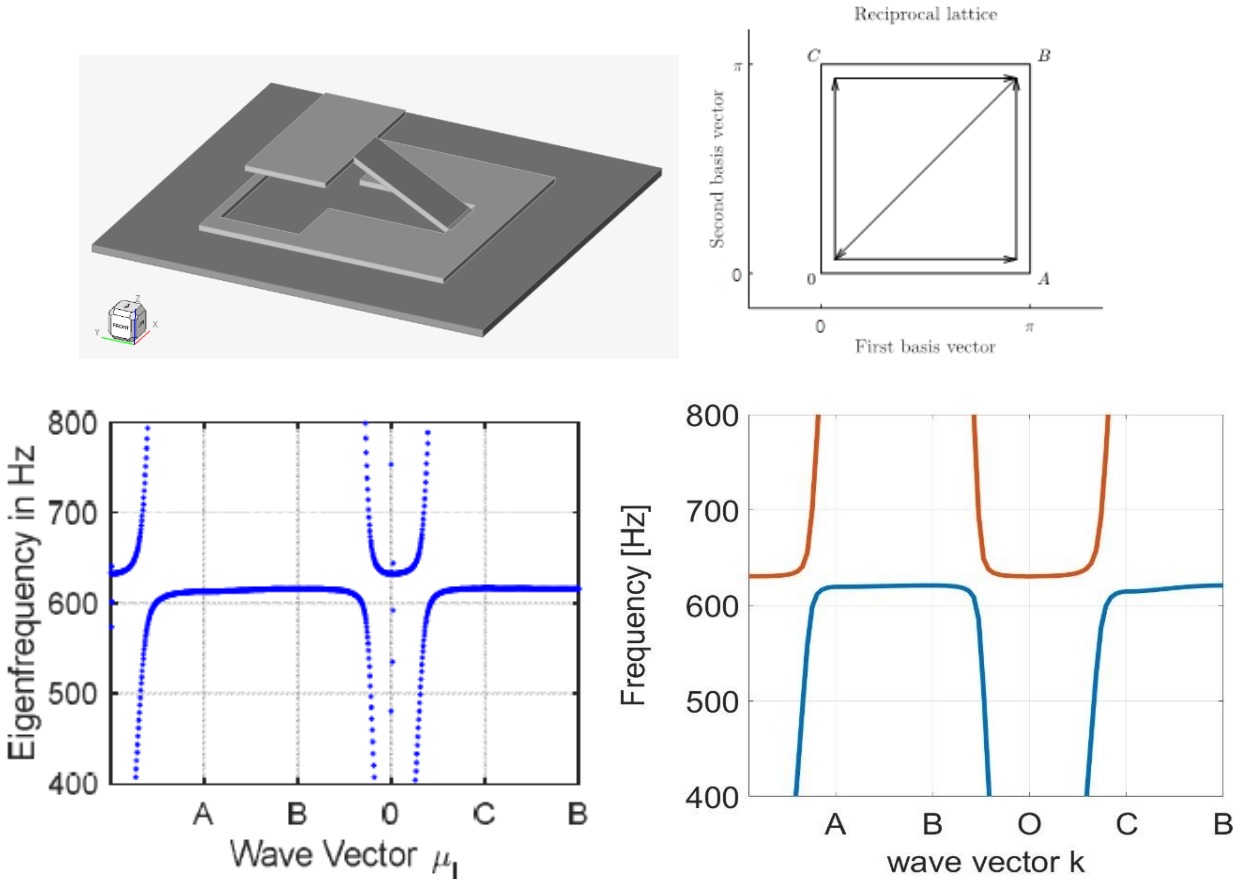

Figure 1: (top-left) T-shaped local resonator metamaterial UC design; (top-right) Irreducible Brillouin Contour; (bottom-left) Dispersion diagram for the metamaterial UC, reported in the [9] compared to the numerical evaluation of this study, whose procedure was to be validated (bottom-right).

The elastic waves that propagate in a waveguide can be considered as the sum of wave modes contributions that are characterized by its own wavelength and frequency. These wave modes are specific of each structure and can be represented by mean of the dispersion curves. The main mathematical tool to understand such a wave propagation is the so-called dispersion diagram [13]. A dispersion diagram (or dispersion relation) for elastic wave propagation, corresponds to the natural frequency f (i.e., the eigenfrequency) of the eigenvalue problem established for the elastic wave equations through the unitary cell under the given periodic boundary conditions (i.e., considering the Bloch theorem [10]), as a function of a wave vector k representing the wavelength in the direction of wave propagation normalized against the physical periodicity (i.e., the size of the unit cells). Studies about wave propagation in periodic, quasi-periodic and aperiodic means can be found in extensively found in the literature, e.g., in [14-20]. These eigenfrequencies clearly depend both on the mechanical properties (like elasticity and density) of the materials making up the unit cell and the geometric arrangement defined by the unit cell structure. Hence, the definition of metamaterials, characterized by their engineered subwavelength structures that give rise to unique mechanical properties

and wave manipulation capabilities not found in naturally occurring materials, making them promising for a wide range of applications in engineering and technology.

In this particular case, the design property of interest was the presence of Band Gaps, ranges of frequencies which are prohibited from propagating mechanical waves through the material. Useful property for vibration and wave attenuation in specific frequency ranges. As it can be noticed in Figure 1, in fact, a stop-band is found from FEM analysis between 615 Hz and 635 Hz. This was proved to shift towards the 580 – 610 Hz range in the experimental validation.

It was the chosen to repeat the very same FEM analysis in [9] so as to validate the algorithm used in this work. The result is shown in Figure 1 (bottom-right picture), which is found to contain the same information as the reference one.

Finally, for the sake of simplicity in further analyses and experimental validation, it was decided to simplify the unit cell considering a metamaterial composed by the aluminum plate alone, while the bending, which was fundamental in order to properly apply the plate on the host structure, was also removed, leaving a simple T-shape cut plate described in the next section.

2.2 Simplified metamaterial and topological considerations

In order to properly engineer the unit cell to tune the stop band to desired values, a parametric geometry was defined. In particular, 4 parameters were considered:

- Periodicity (i.e., the spatial repetition rate of the unit cell, considering Bloch boundary conditions)
- T-element size (with the T element to be simply scaled according to such a parameter)
- Plate material
- Plate thickness

According to such a parameter set, a standard name for the test was defined by the string "*Periodicity / T-size Material – Thickness".* In particular, the reference starting cell was defined as 40/20 Al-0.5, which corresponds to the plane equivalent of the geometry in [9]. Then, starting from this cell which evidences a stop band of size 68 Hz in the range 432-500 Hz (see Figure 2, bottom), univariate variations of the 4 parameters were produced (i.e., one at the time). This clearly not cover the cross-influences of changing different parameters at the same time but was selected so as to derive some simple topological considerations. A full-factorial DOE, which could cover also the presence of cross-effects, will be possibly added in future works.

Anyway, the results are reported in Figures 2 and 3 and in Table 1.

From such a topological analysis the following considerations arise:

- By increasing the periodicity, the stop band reduces in size and in centre frequency until no complete bandgap can be found;
- By increasing the T-size (which for this geometry corresponds to a decrease in the resonant frequency of the T-element), the stop band reduces again in size and in centre frequency;
- By switching from aluminum to steel (i.e., by increasing both the Young's modulus and the density by roughly a factor of 3) the stop band reduces in centre frequency
- By increasing the thickness both the centre frequency and the stop band size are increased.

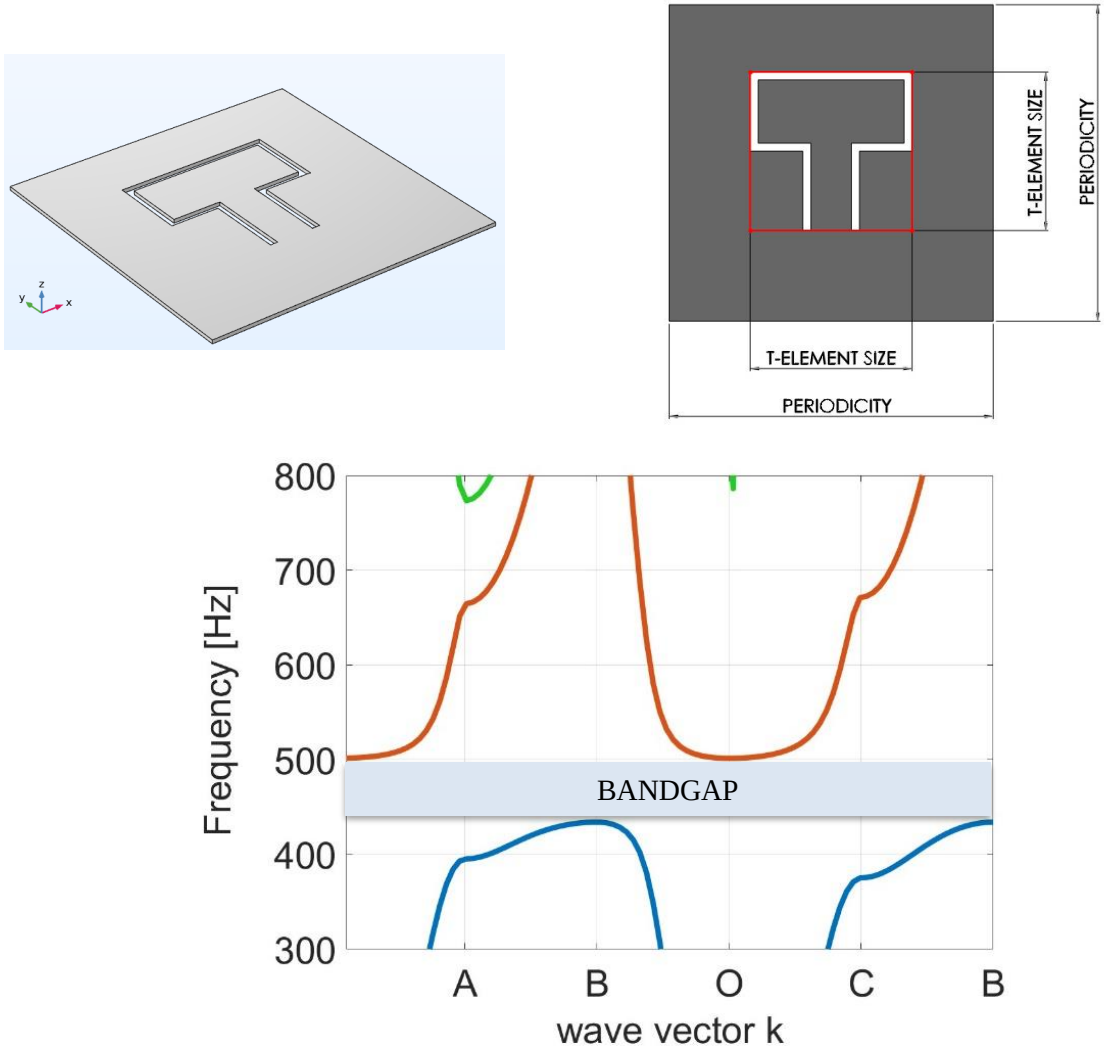

Figure 2: (left) selected unit cell design; (right) selected topological parameters; (bottom) evaluated dispersion diagram for the 40/20 Al-0.5 reference unit cell. Bandgap: 432 - 500 Hz

Table 2– Topological effects on the bandgap in terms of band location and size.

Unit cell design Periodicity/T-size	**Material**	**Thickness [mm]**	**Bandgap [Hz] (band size [Hz])**
40/20	Aluminum	0.5	432-500 (68)
50/20	Aluminum	0.5	411-460 (49)
60/20	Aluminum	0.5	No complete bandgap
30/20	Aluminum	0.5	450-537 (87)
30/15	Aluminum	0.5	1130-1200 (70)
40/35	Aluminum	0.5	232-279 (47)
40/20	Steel	0.5	202-269 (67)
40/20	Steel	1.0	885-1020 (135)

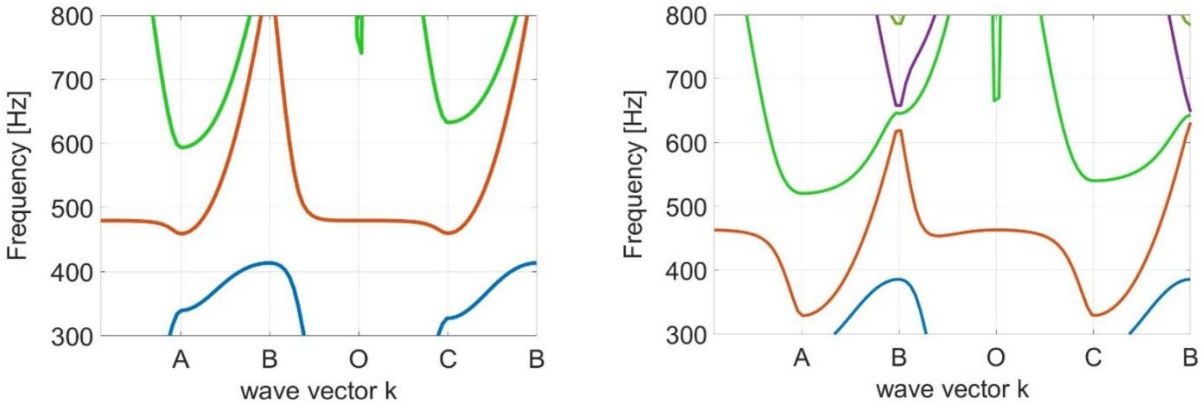

Figure 3: (left) 50/20 Al-0.5 Stopband: 411-460 Hz; (right) 60/20 Al-0.5 Stopband: non-complete

3 Receptance estimation: finite periodic metamaterial

The study of the dispersion relation for the unit cell is certainly crucial for designing metamaterials with specific wave propagation properties and manipulating elastic waves in novel ways. Nevertheless, the assumption of periodic boundary conditions clashes with the need of finite size metamaterial pieces to be used in practical applications. In this regard, a finite periodic metamaterial with physically achievable boundary conditions should be studied.

Given these considerations, a physical plate of size 400 x 400 mm was designed to be laser-cut from a 1 mm thickness steel sheet. The theoretical bandgap for a corresponding infinite plate is 885-1020 Hz, as reported in Table 2. The technical drawing for the realization of such a metal piece is reported in Figure 4. Having in mind to mount the centre of this physical square plate on top of an electrodynamic shaker, a M4 threaded nut was also attached at the centre of the plate.

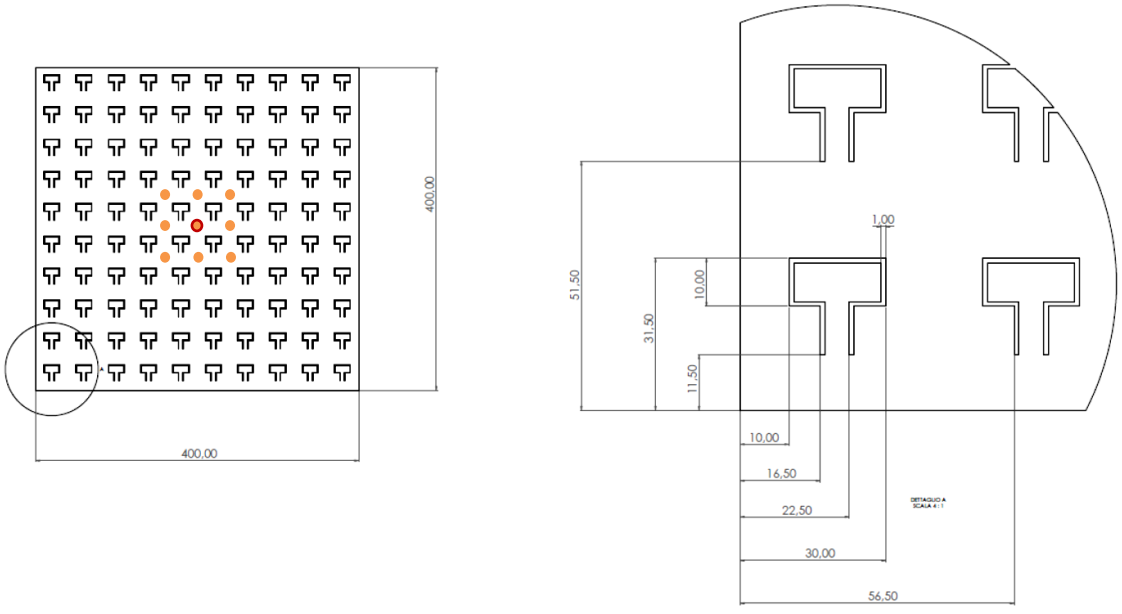

Figure 4: Technical drawing for the realization of a metamaterial sample plate of size 400 x 400 mm laser cut from a 1 mm thickness steel metal sheet. The 9 points for displacement evaluation are highlighted by the orange dots. The central position, which is both a measurement and the forcing point, is circled in red.

Finally, FEM analysis of such a plate was proposed using Calculix free solver and PrePoMax open-source pre and post-processor. Solid elements were selected and a sensitivity analysis for finding a proper mesh size was run, compared to a reference measurement (see section 4.2 for the experimental measurements).

Boundary conditions were selected to simulate a direct mounting on the shaker (i.e., the central nut was bounded to translate only out of the plate plane, while no rotation was allowed; a spring element with low stiffness was also added to limit the out of plane motion).

By adding a unitary harmonic force to the connection nut, a steady state dynamics study was set up, assuming a modal damping of 0.1%. The results in terms of receptances (i.e., the out-of-plane-displacement frequency response to the unit harmonic force) for a grid of 9 points around the centre (see Figure 4) are reported in figure 5.

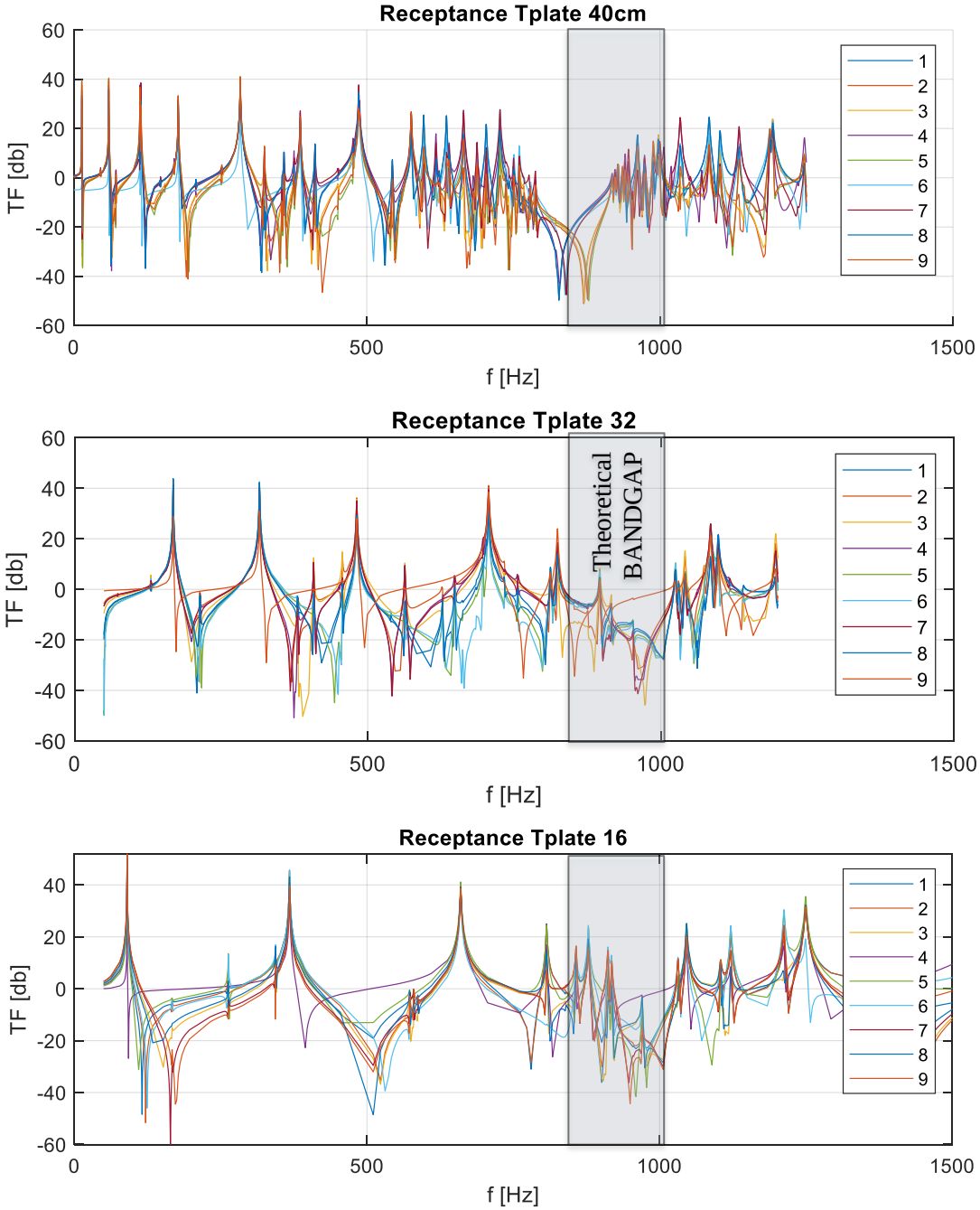

Figure 5: Receptances for metamaterial sample plates of finite size realized from a 1 mm thickness steel metal sheet. The out-of-plane displacement response to the unitary central force, measured in 9 measurement points displayed in Figure 4, are reported. The stop band is visible in the predicted range.

As visible in Figure 5, the 400x400 mm plate evidences a stop band in a region which is contained in the theoretically predicted bandgap from the previous analysis. It is interesting to note that also the 320x320 mm and the 160x160 mm plates show a bandgap within the theoretical range, nevertheless the bandgap is

not exactly the same in the three cases, highlighting an influence of the actual size of the finite plate on the FEM estimated bandgap.

4 Experimental validation

A 400x400 mm metamaterial plate was finally realized by laser cutting the T-shaped unitary cell starting from a 1mm thickness steel sheet. A regular square plate of the same size (i.e., without the T-resonators) was also prepared for testing.

The experimental setup consisted of:

- PCB Piezotronics Model K2007E01 Mini Smart Shaker featuring a 9 kHz frequency range and maximum acceleration of 6.4 g pk with a 0.5 kg payload;
- PCB Piezotronics Model 288D01 ICP® impedance head with a 1-5000 Hz frequency range for both force and acceleration measurements;
- Keyence LK-G high speed, high accuracy CCD laser displacement probe and conditioner, featuring a 4 mm/V sensitivity in a ±10 V (adjustable) range
- Oros OR-38 Data Acquisition system, capable of 8 to 32 synchronous channels acquisitions at 24 bits in a ±40 V adjustable range.

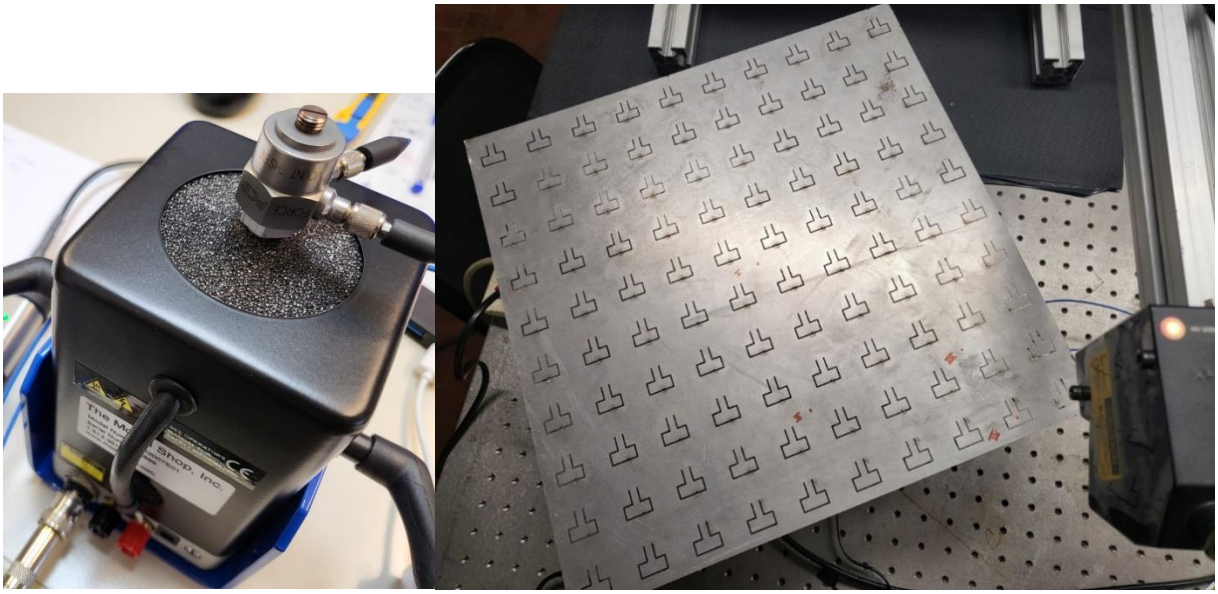

Figure 6: (left) detail of the shaker and impedance head, on top of which the plate was mounted using the M4 visible stud; (right) detail of the laser probe and of the finally tested T-resonators 400x400 mm plate realized by laser-cut from a 1 mm steel sheet. The 4 measurement points selected for the laser displacement acquisitions are reported (i.e., red spots defined by roman numerals I to IV)

A linear sweep from 10 to 1510 Hz in 150s (10Hz/s) was generated by the OR-38 and fed to the shaker. Both the regular plate and the T-shape metamaterial plate were tested. Such measurements were used to validate the simulations run in the previous sections.

4.1 FEM validation on a simple square plate

At first, the Inertance (i.e., the transfer function from the shaker force to the acceleration measured by the impedance head) of the regular plate was used to find rough estimates of the first flexural modes of the plate. The resonance frequencies for the first four visible flexural modes are highlighted in Figure 7.

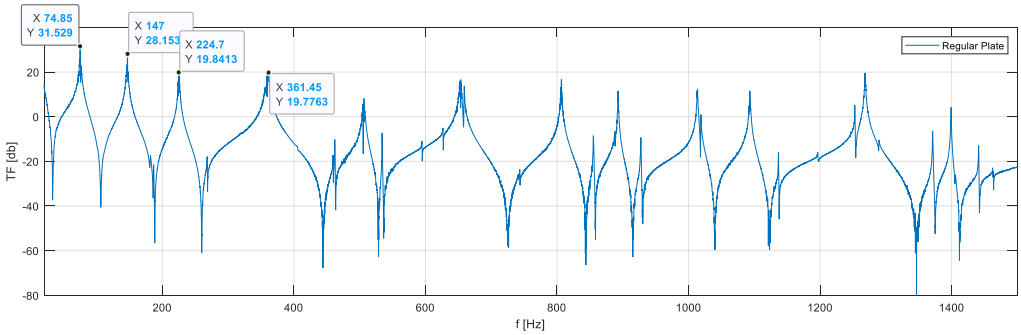

Figure 7: Inertance of the regular 400x400 mm plate: transfer function from the shaker force to the acceleration measured by the impedance head.

A visualization of the corresponding mode-shapes was also produced following the Chladni experiment, which involves the use of fine sand in order to highlight the nodal lines which arise when exciting the plate with a single harmonic at the resonance frequency. These lines can be compared to the same nodal lines which appear in the FEM estimated modal shapes in order to qualitatively evaluate the goodness of the shape estimate, in addition to the goodness in the natural frequency estimation.

In particular, the mesh size of the FEM was selected so as to produce the sufficiently similar results which are reported in Figure 8 and in Table 3. Notice that for particularly small damping factors as the one involved in the present study (i.e., no added damping), the resonance frequency and the natural frequency can be practically regarded as one. Also, it is relevant to consider that no parametric update was done on the material properties which were left to the initial generic values of 210 GPa for Young's modulus and 7800 kg/m^3 for the density.

Table 3 – Goodness of the FEM 400x400 mm regular square plate compared to the measured resonance frequencies visible in figure 7.

FEM mode #	FEM eigenfrequency [Hz]	Resonance freq. as estimated from measurements [Hz]	% error
9	71.8	75	4.3 %
14	137	147	6.8 %
22	221	224.7	1.6 %
31	347	361.5	4 %

It is relevant to point out that for the regular plate an element size range of 0.1-5 mm was enough to produce acceptable results. The same parameter was used for the T-cut metamaterial plate, but to better fit the small 1 mm cuts that were needed to create the resonators (see Figure 4), a way larger number of elements was produced by the mesher. This led to numerical simulations with a higher computational burden, as the number of nodes/elements increased from 90528/44782 to 577515/270808 (i.e., roughly a factor of 5), and the time to solution for modal analysis alone (excluding the steady state dynamics step) increased accordingly, up to 3378.6 s for the 400x400 mm T-resonator plate on a PC with 32 GB of ram and a i7-7700 processor (N.B., no parallelization option was selected).

It is interesting to point out that the number of eigenmodes in the range 1-1250 Hz also increased from 81 to 175 while switching from the regular square plate to the T-resonator metamaterial plate. This is due to the fact that, even if the lower frequency modes were not too much affected by the T-cuts, in the frequency range indicated as the theoretical bandgap many new mode shapes were present, with clusters of resonators activated.

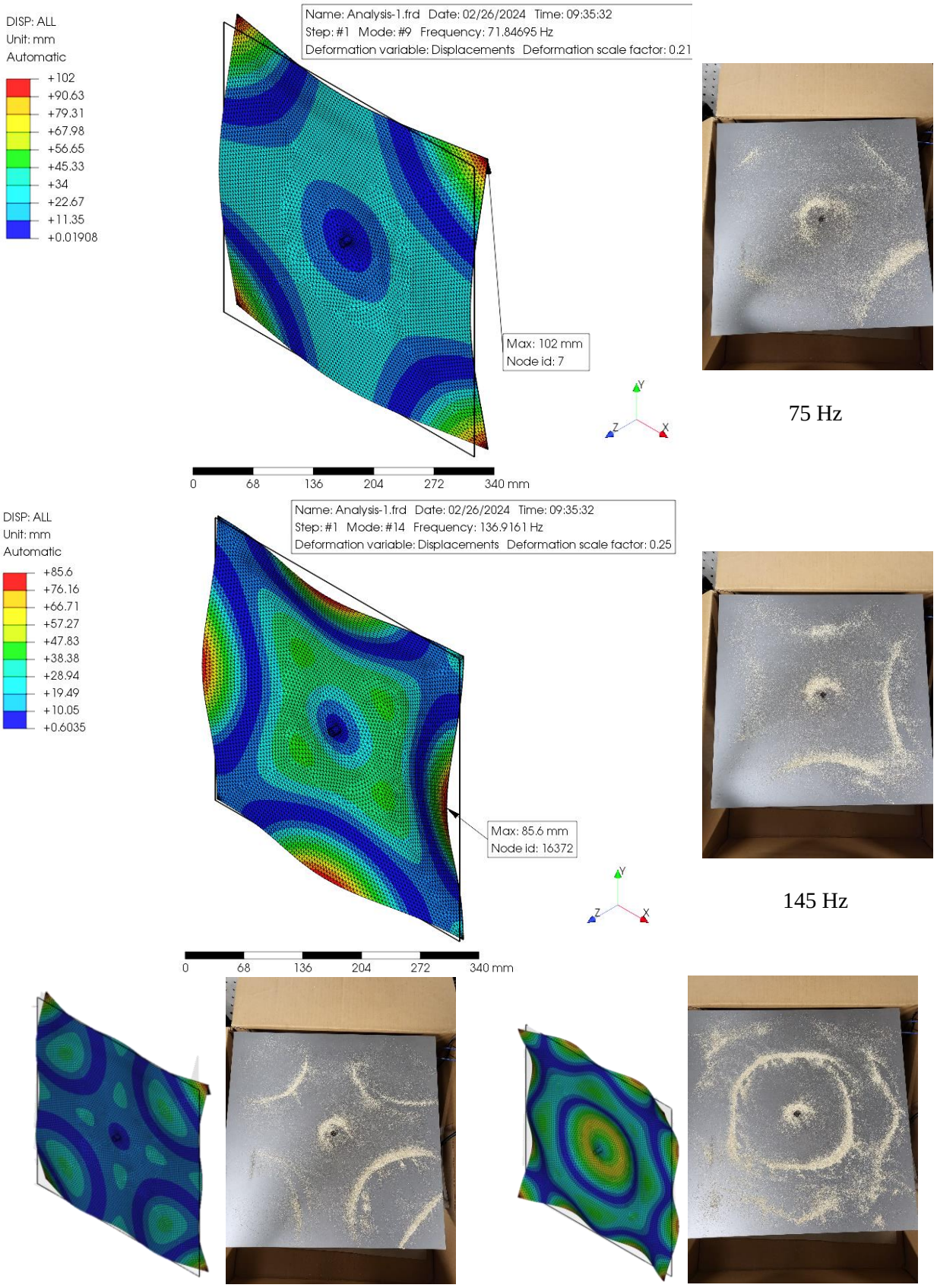

Figure 8: FEM derived modal shapes Vs Chladni experiment using fine sand and exciting with a harmonic force at the resonance frequency (reported below each photo).

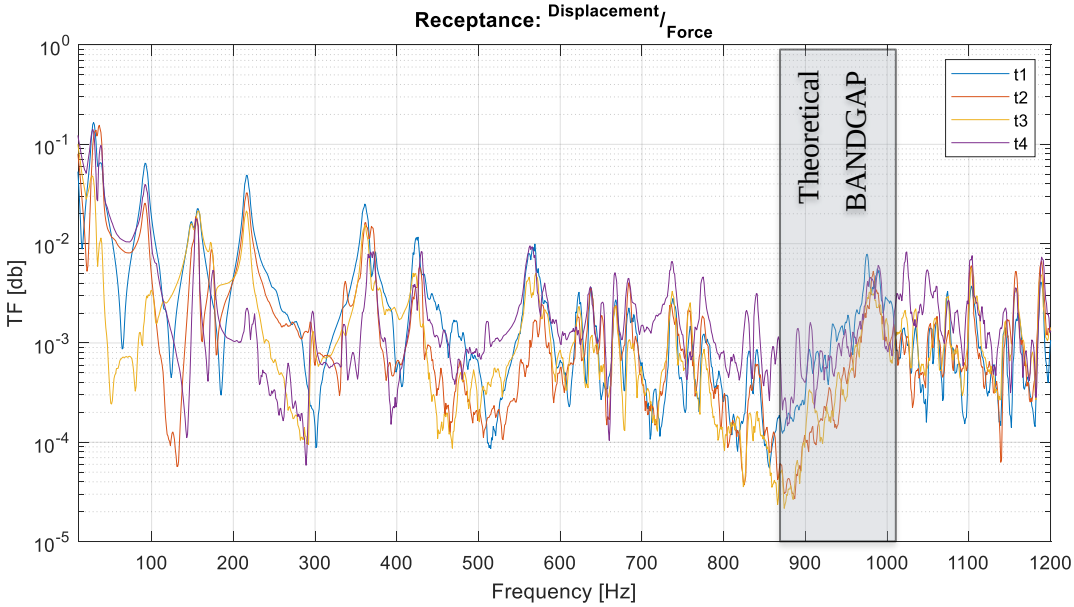

Figure 9: Estimated receptances for laser measurements in spots I to IV (i.e., t1 to t4) given the sweep excitation. Notice that t1 to t3 are on the plate, while t4 is on a resonator. A stop band is clearly visible in the 870-900 Hz range, which almost falls within the theoretically estimated bandgap region (i.e., 885-1020 Hz, as reported in Table 2).

4.2 T-resonators finite plate analysis in the frequency domain: experimental results

Finally, the FEM procedure was compared also on the T-resonator 400x400 mm finite steel plate, 1mm thick. The experimental laser measurements in spots I to IV in Figure 6 were used together with the measured force during the sweep excitation in order to find estimates of the displacement to force transfer function, defined as Receptance (i.e., t1 to t4 curves in Figure 9). Notice that t1 to t3 are on the plate, while t4 is on a resonator. A stop band is clearly visible for t1 to t3 in the 870-900 Hz range, which partially falls within the theoretically estimated bandgap region (i.e., 885-1020 Hz, as reported in Table 2). It is interesting to note that, focusing on the resonator response (i.e., t4) resonances are visible around 900 Hz, confirming the presence of many additional modes related to the “activation” of clusters of T-resonators.

5 Conclusions

To summarize, in this paper a dynamic analysis of elastic metamaterials for industrial applications, with a particular focus on NVH noise reduction for vehicles, was set up based on similar literature contributions. In particular, the work started by the numerical FEM analysis of a single unit-cell with periodic boundary conditions, and some evidence of the topological influence of the unit cell geometry on the band-gap was derived. Secondly, a finite plate was analysed, with physically sound boundary conditions. This showed the influence of the actual finite size on the bandgap, which was present in a reduced band size. Finally, experimental tests on real laser-cut steel plates were used to validate the proposed simulations, confirming the presence of a stop-band in a range not far from the theoretically predicted bandgap and making such a metamaterial promising for a wide range of applications in engineering and technology.

In particular, future works will involve the application of such materials in the field of aerospace qualification testing, with a particular focus on pyroshock testing [21], where the ability of changing the receptance of a finite plate can be valuable for tuning the shock response spectra so as to match the

qualification requirements. This could bring benefits also to the field of diagnostics, where the transmission path to vibration monitoring sensors could be shaped by using particular metamaterials rather than relying only on wise sensor placement ([22-25]).

References

[1] L. Y. L. Ang, Y. K. Koh and H. P. Lee, "Acoustic Metamaterials: A Potential for Cabin Noise Control in Automobiles and Armored Vehicles," *International Journal of Applied Mechanics*, vol. 8, no. 5, 2016.

[2] M. Koichi and K. Yuhei, "3D printing of fiber composite sandwich metamaterial with spiral resonators for attenuation of low-frequency structural vibration," *Composites Part A: Applied Science and Manufacturing*, vol. 172, no. 107594, 2023.

[3] I. Raza and H. Mohammad, "Additive manufacturing of locally resonant metamaterials," Ph.D. dissertation, Imperial College London, 2017.

[4] J. Yupei, H. Guobiao, T. Lihua and C. A. Kean, "Band Gap Formation in Metamaterial Beam With Torsional Local Resonators for Vibration Suppression.," in *Proceedings of the ASME 2020 Conference on Smart Materials, Adaptive Structures and Intelligent Systems. ASME 2020 Conference on Smart Materials, Adaptive Structures and Intelligent Systems*, 2020.

[5] C. Nerse, R. Schadeberg and S. Oberst, "Novel resonator geometry for easily manufactured tunable locally resonant metamaterial," in *2021 Annual Conference of the Australian Acoustical Society 2021: Making Waves, AAS 2021*, Woolongong, 2021.

[6] N. F. Melo, C. Claeys, E. Deckers, B. Pluymers and W. Desmet, "Dynamic Metamaterials for Structural Stopband Creation," in *SAE Int. J. Passeng. Cars - Mech. Syst., 9th International Styrian Noise, Vibration & Harshness Congress: The European Automotive Noise Conference, 9(3)*: 2016, pp. 1013-1019.

[7] L. Sangiuliano, C. Claeys, E. Deckers, B. Pluymers and W. Desmet, "Force Isolation by Locally Resonant Metamaterials to Reduce NVH," SAE, 2018.

[8] M. Yuxuan, C. Lihua, Z. Mengjiao and Z. Yadi, "A Local Resonance Metamaterial For Vibration Reduction," in *2021 4th World Conference on Mechanical Engineering and Intelligent Manufacturing (WCMEIM), Shanghai, China, 12-14 November 2021*.

[9] S. Riess et al., "Vibroacoustic Metamaterials for enhanced acoustic Behavior of Vehicle Doors," in *Fifteenth International Congress on Artificial Materials for Novel Wave Phenomena (Metamaterials), 2021, NYC, NY, USA*, 2021, pp. 374-376.

[10] L. Brillouin, *Wave Propagation in Periodic Structures*. 2nd, McGraw-Hill Book Company, 1946.

[11] A. Melnikov, M. Hanke and S. Marburg, "Dispersion Curves of Elastic Metamaterials and Sonic Crystals with ANSYS," *2018, CASCON Conference*, Leipzig.

[12] R. Langley, "A Note On The Force Boundary Conditions For Two-Dimensional Periodic Structures With Corner Freedoms," *Journal of Sound and Vibration*, vol. 167, no. 2, pp. 377-381, 1993.

[13] E. Groth, I. Iturrioz and T. Clarke, "The dispersion curve applied in guided wave propagation in prismatic rods," *Latin American Journal of Solids and Structures*, vol. 15, no. 6, 2018.

[14] J.-M. Mencik and D. Duhamel, "DYNAMIC ANALYSIS OF PERIODIC STRUCTURES AND METAMATERIALS VIA WAVE APPROACHES AND FINITE ELEMENT PROCEDURES," in *8th International Conference on Computational Methods in Structural Dynamics and Earthquake Engineering Methods in Structural Dynamics and Earthquake Engineering, Athens, Greece, 2021*, pp. 42–62.

[15] S. D. Lust, P. P. Friedmann, andd O. O. Bendiksen, "Free and forced response of multi-span beams and multi-bay trusses with localized modes," *Journal of Sound and Vibration*, vol. 180, no. 2, pp. 313–332, February 1995.

[16] D. J. Mead and S. Parthan, "Free wave propagation in two-dimensional periodic plates," *Journal of Sound and Vibration*, vol. 64, no. 3, pp. 325–348, June 1979.

[17] E. E. Ungar, "Steady-State Responses of One-Dimensional Periodic Flexural Systems," *The Journal of the Acoustical Society of America*, vol. 39, no. 5A, pp. 887–894, May 1966.

[18] B. L. Clarkson and R. D. Ford, "The Response of a Typical Aircraft Structure to Jet Noise," *The Aeronautical Journal*, vol. 66, no. 613, pp. 31–40, January 1962.

[19] G. SenGupta, "Vibration of Periodic Structures," *The Shock and Vibration Digest*, vol. 12, no. 3, pp. 17–31, March 1980.

[20] D. J. Mead, "Vibration Response and Wave Propagation in Periodic Structures," *Journal of Engineering for Industry*, vol. 93, no. 3, pp. 783–792, August 1971.

[21] L. Viale, et al., "On pyroshock tests for aerospace equipment qualification: A comprehensive parametric model for the simulation and the design of pyroshock test facilities," *International Journal of Impact Engineering*, vol. 180, 2023.

[22] A. P. Daga, et al., "Big Data management: A Vibration Monitoring point of view," in *Proceedings of 2020 IEEE International Workshop on Metrology for Industry 4.0 & IoT, IEEE*, pp. 548–553, 2020.

[23] L. Viale, et al., "From Novelty Detection to a Genetic Algorithm Optimized Classification for the Diagnosis of a SCADA-Equipped Complex Machine," *MACHINES*. Vol. 10, 2022.

[24] L. Viale, et al., "Dimensionality Reduction Methods of a Clustered Dataset for the Diagnosis of a SCADA-Equipped Complex Machine," *MACHINES.* vol. 11, 2023.

[25] L. Viale, et al., "Least squares smoothed k-nearest neighbors online prediction of the remaining useful life of a NASA turbofan," *MECHANICAL SYSTEMS AND SIGNAL PROCESSING*, vol. 190, 2023.